

Supporting Information for
Computational design of a red fluorophore ligase
for site-specific protein labeling in living cells

Daniel S. Liu¹, Lucas G. Nivón², Florian Richter^{2,3,4}, Peter J. Goldman¹, Thomas J. Deerinck⁵,
Jennifer Z. Yao¹, Douglas Richardson⁶, William S. Phipps¹, Anne Z. Ye¹, Mark H. Ellisman^{5,7},
Catherine L. Drennan^{1,8,9}, David Baker^{2,10}, and Alice Y. Ting^{1*}

¹Department of Chemistry, Massachusetts Institute of Technology, Cambridge, Massachusetts 02139, USA

²Department of Biochemistry, University of Washington, Seattle, Washington 98195, USA

³Graduate program in Biological Physics, Structure and Design, University of Washington, Seattle, Washington 98195, USA

⁴Present address: Institute of Biology, Humboldt-Universität zu Berlin, Germany

⁵National Center for Microscopy and Imaging Research, Center for Research on Biological Systems, University of California at San Diego, La Jolla, California 92093, USA

⁶Department of NanoBiophotonics, Max Planck Institute for Biophysical Chemistry, Göttingen, Germany

⁷Department of Neurosciences, University of California at San Diego, La Jolla, California 92093, USA

⁸Department of Biology, Massachusetts Institute of Technology, Cambridge, Massachusetts 02139, USA

⁹Howard Hughes Medical Institute, Massachusetts Institute of Technology, Cambridge, Massachusetts 02139, USA

¹⁰Howard Hughes Medical Institute, University of Washington, Seattle, Washington 98195, USA

*To whom correspondence should be addressed. Email: ating@mit.edu

Contents

Figures S1 – 11	2
Table S1	14
Supporting Methods.....	15
References.....	27

Supporting Figures

A

Resorufin 1		W37 mutation →							
		none	A	T	V	I	G	S	L
E20 mutation ↓	none	N.D.	N.D.	N.D.	N.D.	N.D.	N.D.	N.D.	N.D.
	G		N.D.	N.D.		N.D.			
	A	N.D.	N.D.	N.D.	N.D.				
	S		N.D.	N.D.	N.D.	N.D.			

Resorufin 2		W37 mutation →							
		none	A	T	V	I	G	S	L
E20 mutation ↓	none	N.D.	N.D.	N.D.	20	N.D.	N.D.	N.D.	N.D.
	G		N.D.	N.D.		N.D.			
	A	N.D.	N.D.	N.D.	N.D.				
	S		10	N.D.	N.D.	10			

B

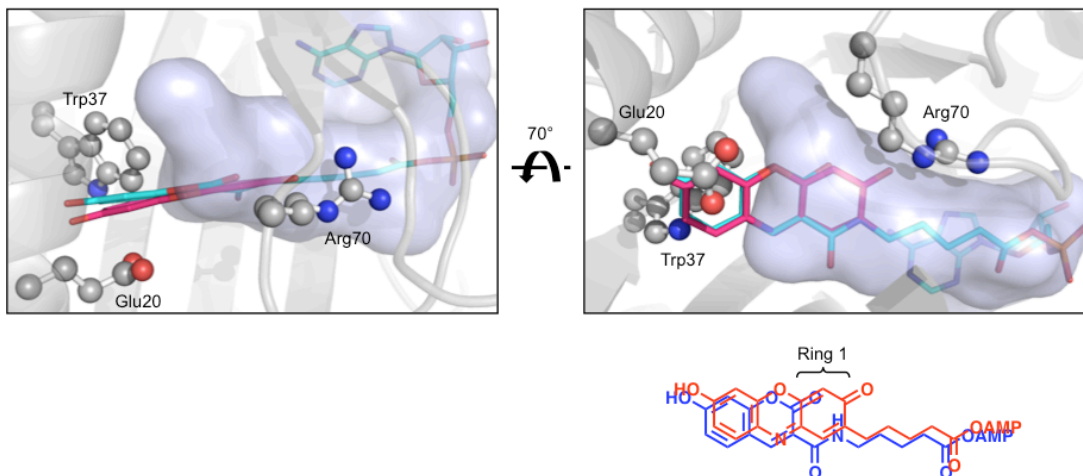


Fig. S1. Screening of wild-type and nineteen Glu20 and Trp37 single and double mutants of LplA for resorufin ligation activity. **(A)** HPLC assays were performed with 2 μ M enzyme, 500 μ M resorufin and 200 μ M LAP peptide for 4 hr. Percent conversion to resorufin-LAP product conjugate, rounded to the nearest ten, is reported in each cell. N.D. denotes “not detected”, where 3% conversion was the approximate detection limit. Grey-shaded cells were not tested. Only three conditions (shaded pink) produced detectable product. **(B)** Cut-away views of the wild-type LplA crystal structure (PDB ID: 3A7R) (1) with resorufin 2-AMP (shown in pink sticks) and coumarin-AMP (shown in cyan sticks) modeled into the substrate binding pocket. The resorufin and coumarin molecules are modeled to be approximately co-planar with the dithiolane ring of lipoic acid in 3A7R. The inner surface of the substrate binding tunnel is shown in blue and is bounded by Glu20, Trp37, and Arg70 sidechains (shown in grey ball-and-sticks). Overlay of resorufin 2-AMP (red) and coumarin (blue) chemical structures with slight offset is shown below the right panel. Ring 1 of resorufin is indicated.

A

Resorufin 2-AMP binding energy	Rosetta score	Sequence ID	Design name	LplA residue number						
				17	20	70	85	122	147	149
		Wild-type		L	E	R	G	D	F	H
-3.47	-516.92	1	16_92	G	E	S	G	D	F	S
-3.07	-503.48	2	7_33	L	A	R	G	D	A	G
-3.04	-504.54	2	7_98	L	A	R	G	D	A	G
-3.03	-506.48	2	15_81	L	A	R	G	D	A	G
-2.95	-505.82	2	15_51	L	A	R	G	D	A	G
-2.94	-509.09	2	7_96	L	A	R	G	D	A	G
-2.93	-504.26	2	15_8	L	A	R	G	D	A	G
-2.92	-505.96	2	7_17	L	A	R	G	D	A	G
-2.92	-504.25	2	15_32	L	A	R	G	D	A	G
-2.91	-506.81	2	7_73	L	A	R	G	D	A	G

B

Resorufin 2-AMP binding energy of best design	Rosetta score	Sequence ID	Occurrence in top 216 designs	17	20	70	85	122	147	149
				L	E	R	G	D	F	H
		Wild-type		L	E	R	G	D	F	H
- 3.47	-516.92	1	1	G	E	S	G	D	F	S
- 3.07	-503.48	2	190	L	A	R	G	D	A	G
- 2.91	-509.38	3	1	L	A	R	G	A	A	G
- 2.63	-503.88	4	11	L	A	R	G	D	G	G
- 2.59	-506.51	5	1	L	A	R	G	D	S	G
- 2.54	-514.29	6	1	L	E	R	G	D	A	G
- 2.49	-504.36	7	9	L	E	R	C	D	A	G
- 2.15	-509.82	8	1	L	E	R	G	D	G	G
- 1.77	-524.23	9	1	L	A	T	G	D	A	G

Fig. S2. Results of Rosetta computational design. **(A)** From 1600 independent Rosetta designs, the top half in overall Rosetta score were intersected with: (i) the top half in quality of atom packing, (ii) the top half in satisfying buried non-polar residues, and (iii) the top 20% by resorufin 2-AMP interaction energy. This gave a compacted set of 216 designs, the top 10 of which are shown here, ranked by resorufin 2-AMP binding energy. This table lists all top designs (which may share the same amino acid sequence but differ in conformations). Red shading highlights mutations with respect to the wild-type LplA sequence. Design was carried out with a conservative bias (a penalty was given to deviations from the wild-type sequence). The 2nd through 10th designs have the same amino acid sequence (resorufin ligase used in this work), but they possess slightly different conformations and hence different Rosetta scores. The designs were highly convergent on the resorufin ligase, which represented 190 out of the 216 top designs. The highest ranked sequence, 16_92, was inactive for both lipoic acid and resorufin 2 ligation in an HPLC assay (data not shown). **(B)** Altogether 9 unique amino acid sequences were discovered from the 1600 designs, shown here ranked by resorufin 2-AMP binding energy of the best design representing each sequence. Units for binding energy and Rosetta score are Rosetta Energy Units (REU).

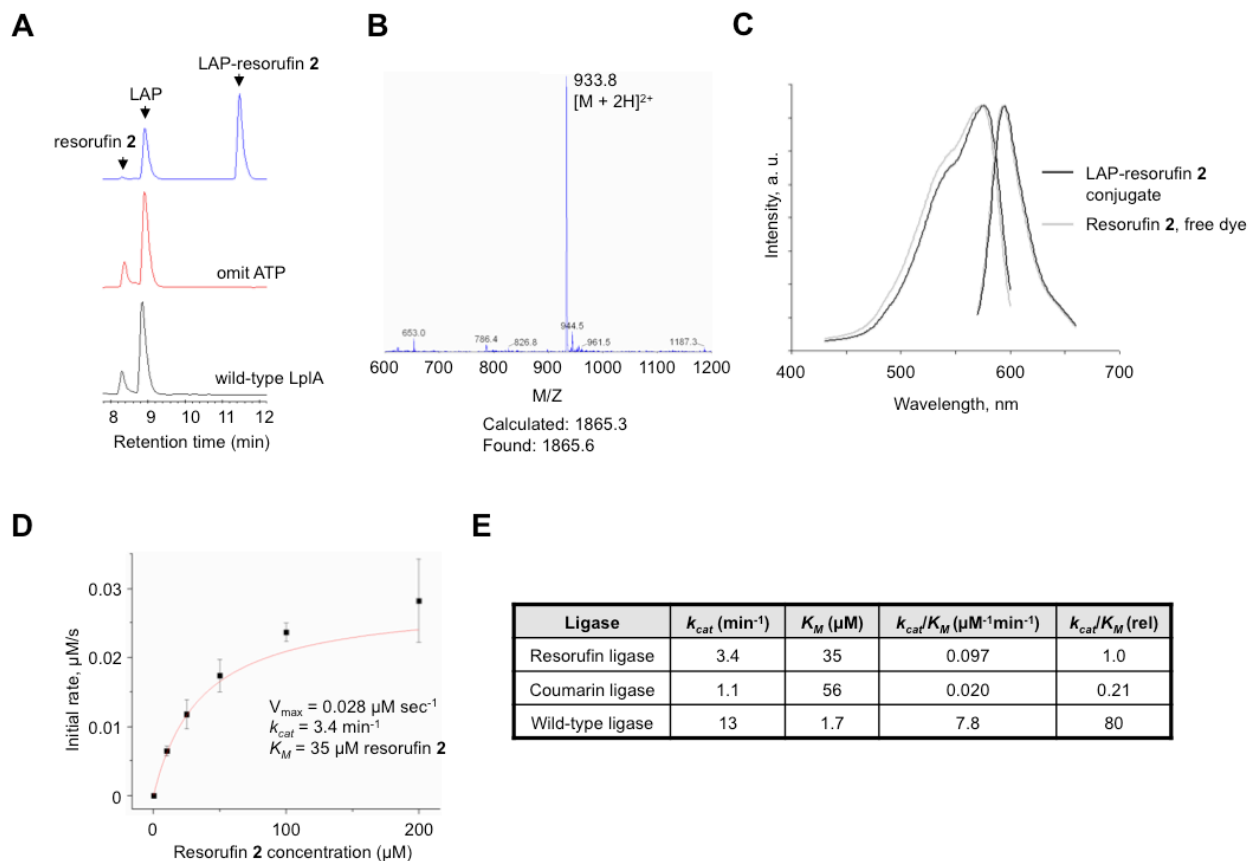


Fig. S3. *In vitro* characterization of resorufin ligation. **(A)** HPLC analysis of resorufin **2** ligation to LAP peptide (blue trace). Negative controls are shown with ATP omitted from the ligation reaction (red trace), or with resorufin ligase replaced by wild-type LplA (black trace). **(B)** The LAP-resorufin **2** product peak from **(A)** was analyzed by mass spectrometry to confirm its identity. **(C)** Excitation and emission spectra of resorufin **2** and resorufin **2**-LAP conjugate. **(D)** Michaelis-Menten kinetic parameters of resorufin ligation were measured by HPLC. The plot shows the initial rates as a function of resorufin **2** concentration. The enzyme was supplied at 0.5 μM . **(E)** Table of kinetic parameters of resorufin ligation, compared to coumarin ligation by coumarin ligase (2) and liponic acid ligation by wild-type enzyme (3).

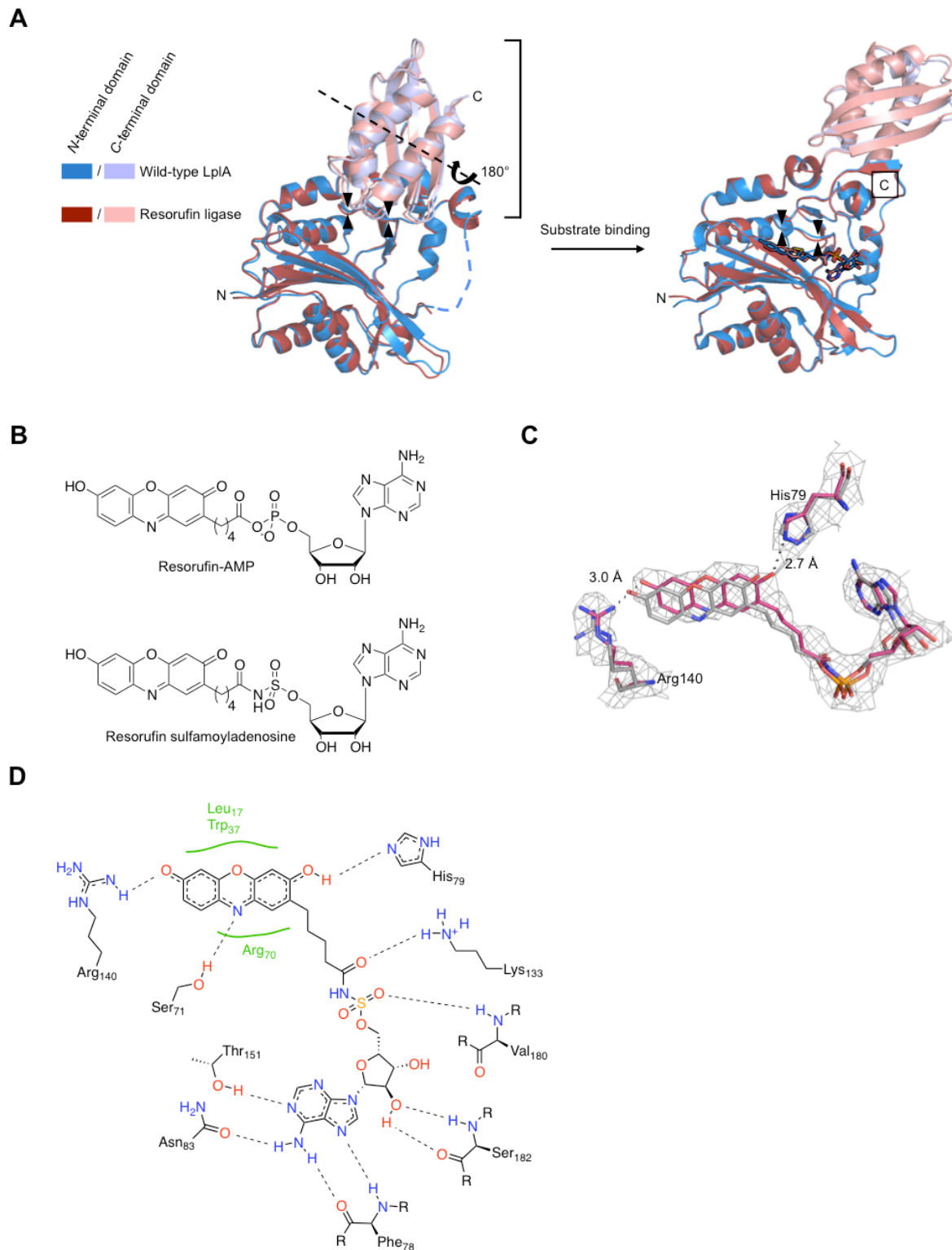


Fig. S4. Resorufin ligase crystal structure and comparison to the Rosetta design and wild-type LplA. (A) Global conformational transitions of resorufin ligase and wild-type LplA. Substrate binding causes wild-type LplA (blue/light blue ribbons) to undergo large-scale rotation of its C-terminal domain (1). Identical changes are seen when comparing the apo structure of resorufin

ligase (left, red/pink ribbons, 2.2 Å resolution) to the substrate-bound structure (3.5 Å resolution, right). Bound adenylate ester substrates are shown in sticks. The *N*- and *C*-terminal ends of both proteins are labeled. The lipoate/resorufin binding loops (residues 70 to 75) are indicated with arrowheads. The disordered and invisible adenylate binding loops (residues 175 to 182) are shown as a blue dashed line. Upon substrate adenylate ester binding, the lipoate/resorufin binding loops clamp down, the adenylate binding loops become ordered, and the *C*-terminal domains undergo an $\sim 180^\circ$ rotation. The wild-type LplA apo and substrate-bound structures are taken from PDB 1X2H (4) and 3A7R (1), respectively. **(B)** The chemical structures of resorufin-AMP (top, the natural substrate intermediate for resorufin ligase), and resorufin sulfamoyladenosine (bottom, a non-hydrolyzable analog of resorufin-AMP). **(C)** Active site detail for the designed (grey sticks) and crystal (pink sticks) structures of resorufin ligase. The resorufin moiety is shifted by ~ 1 Å compared to the design, which allows both phenolic positions of resorufin to form hydrogen bonds with Arg140 and His79 side chains (distances shown). In the design the *cis* phenol is beyond hydrogen bonding distance from His79. The $2F_o - F_c$ electron densities in the crystal structure are shown in grey mesh and contoured to 1.0σ . **(D)** Contacts of resorufin sulfamoyladenosine with nearby residues. Hydrophobic interactions are indicated by green curves.

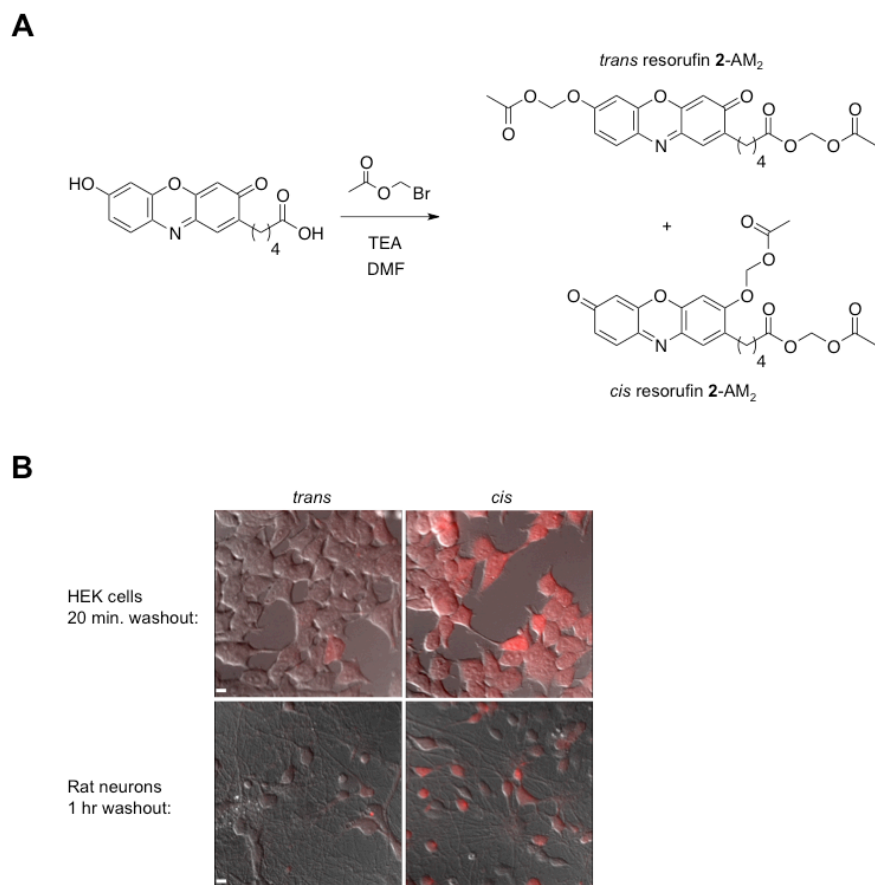


Fig. S5. Resorufin 2-AM₂ regioisomers have different intracellular retention properties. **(A)** Acidic group masking of resorufin 2 with acetoxymethyl (AM) bromide produces two regioisomers (*trans* and *cis*). TEA, triethylamine; DMF, *N,N*-dimethylformamide. **(B)** Testing in cells shows that both regioisomers enter HEK cells (top) and cultured rat neurons (bottom) efficiently, but *trans* resorufin 2-AM₂ gives cleaner washout (lower background) than *cis* resorufin 2-AM₂. Resorufin fluorescence is shown in red and overlaid with DIC. Scale bars, 10 μ m.

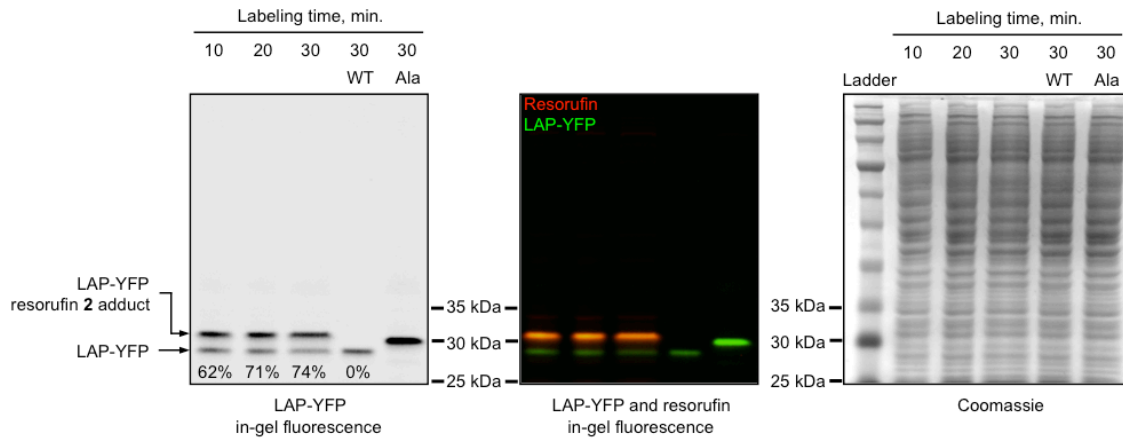


Fig. S6. Determination of resorufin ligation yield inside living cells by a gel-shift assay. HEK cells expressing LAP-YFP and resorufin ligase were labeled with 5 μ M resorufin 2-AM₂ for the indicated duration, followed by 45 min. of dye washout. Cells were then lysed and the clarified lysate was resolved by SDS-PAGE without sample boiling. Visualization of LAP-YFP in-gel fluorescence (left panel) shows an upward shift upon resorufin attachment. Densitometry of the bands at 10, 20, and 30 min. labeling time revealed labeling yields indicated below. Labeling yields were not proportional to labeling time probably because labeling continued during the 45-min. dye washout period. Negative controls with wild-type ligase and Lys→Ala mutation in LAP are shown. Samples were not boiled prior to loading and the Ala mutant of LAP has a different mobility presumably due to charge density difference compared to LAP. Resorufin ligation to the upper band was confirmed by visualization of resorufin fluorescence in the same gel, shown overlaid with LAP-YFP fluorescence in the second panel. The coomassie stain of this gel is shown in the third panel.

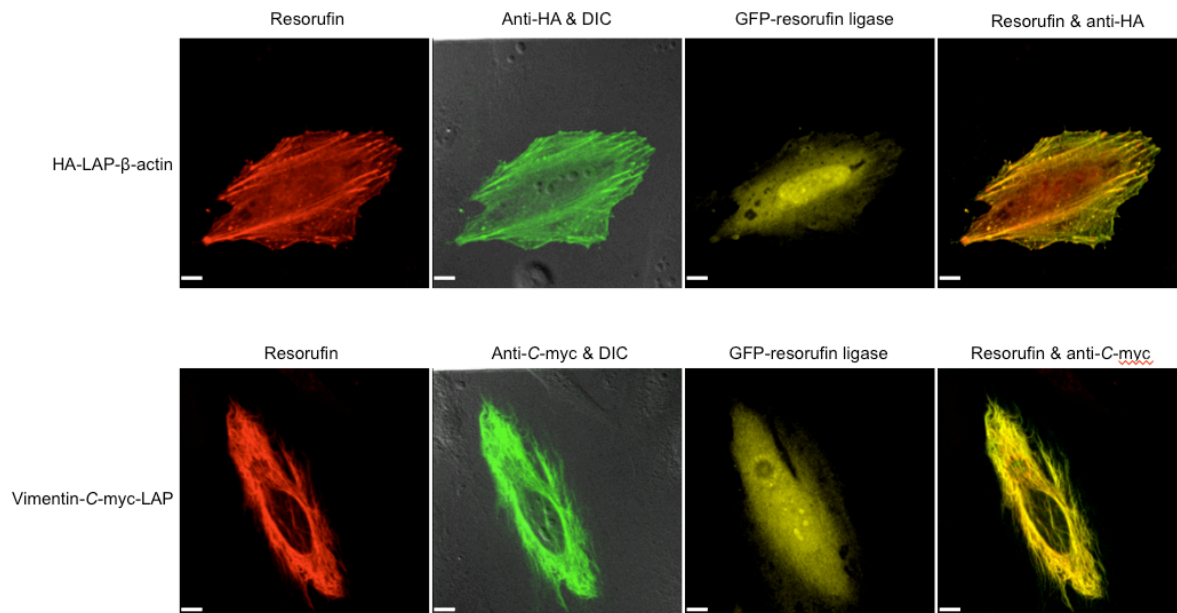


Fig. S7. Comparison of resorufin labeling and immunofluorescence staining for actin and vimentin. Living HeLa cells expressing GFP-tagged resorufin ligase (yellow, third column) and HA-LAP-β-actin or vimentin-LAP-C-myc were labeled with 5 μM resorufin 2-AM₂ (red, first column) for 30 min. followed by 45 min. of dye washout. After cell fixation, LAP-β-actin was detected by anti-HA immunofluorescence staining, and vimentin-LAP was detected by anti-C-myc immunofluorescence staining (green, overlaid with DIC in second column). Scale bars, 10 μm.

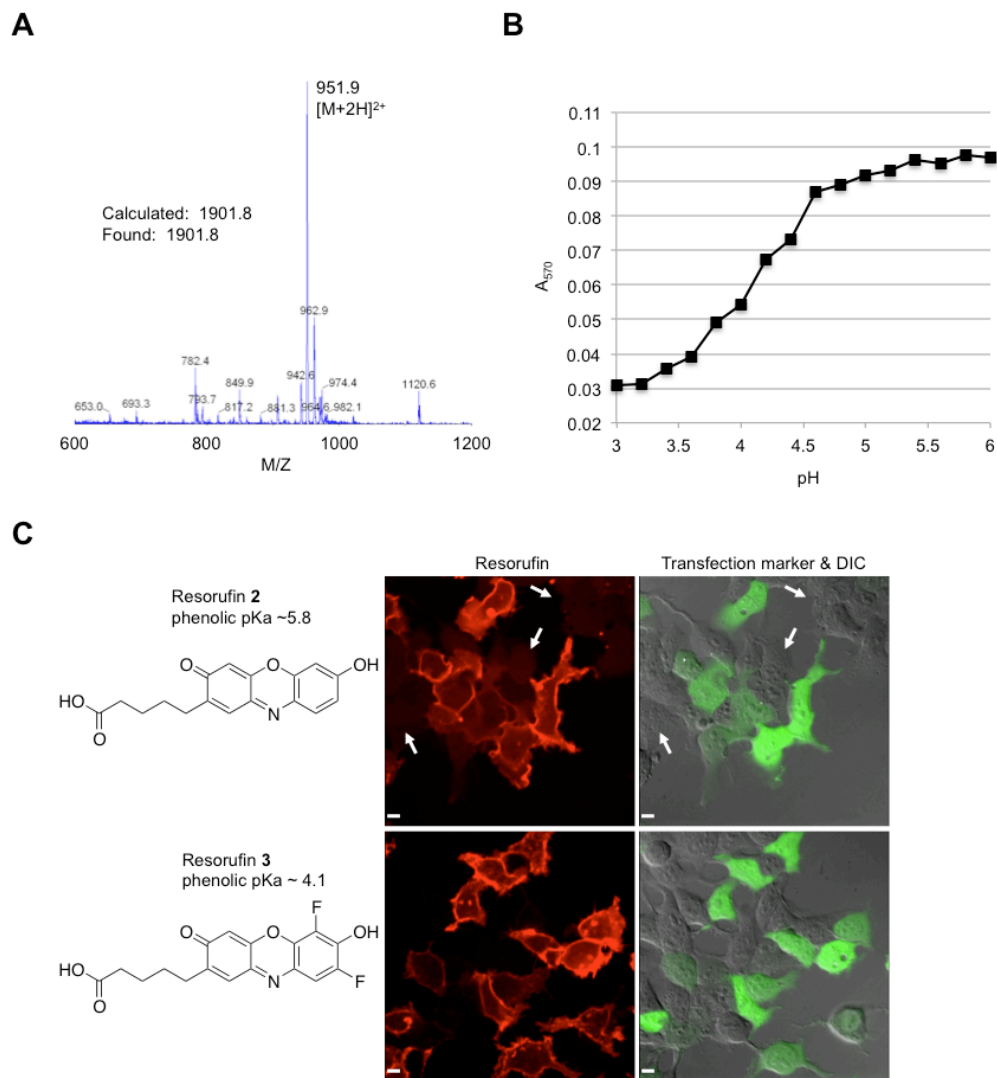


Fig. S8. Improved cell surface labeling with fluorinated resorufin. **(A)** Resorufin ligase-catalyzed *in vitro* ligation of resorufin **3** onto LAP was confirmed by mass spectrometry. **(B)** The absorbance of resorufin **3** at 570 nm was measured from pH 3 to 6. Protonation of the resorufin **3** phenolate causes a drop in A_{570} , allowing the determination of its pKa to be ~4.1. **(C)** Comparison of resorufin substrates for cell surface labeling. HEK cells expressing LAP-tagged low-density lipoprotein receptor and a fluorescent protein transfection marker (shown in green and overlaid with DIC on the right) were labeled with either resorufin **2** (top row) or resorufin **3** (bottom row) using exogenously supplied resorufin ligase and imaged immediately after three quick rinses. Labeling with resorufin **2** generated a faint intracellular background, even in untransfected cells (indicated by arrows) due to slight membrane permeability of the dye. In contrast, labeling with the less permeable resorufin **3** did not generate intracellular background and facilitated more sensitive detection of endocytosed protein pools.

A

Acceptor moiety	Sequence
E2p	...ITVEGD <u>K</u> ASMEVPAP...
LAP	GFEID <u>K</u> VMYDLDA
LAP-F	GFEID <u>K</u> VFYDLDA

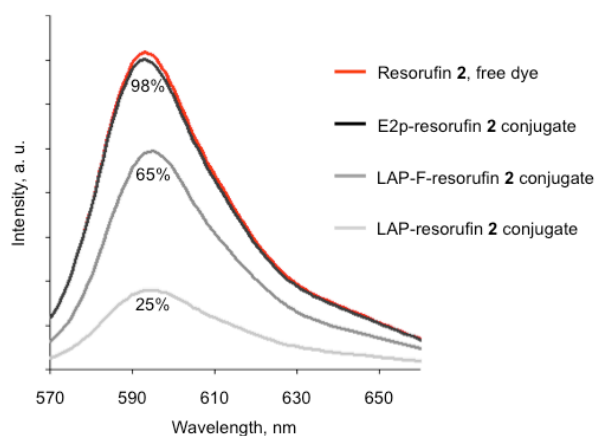
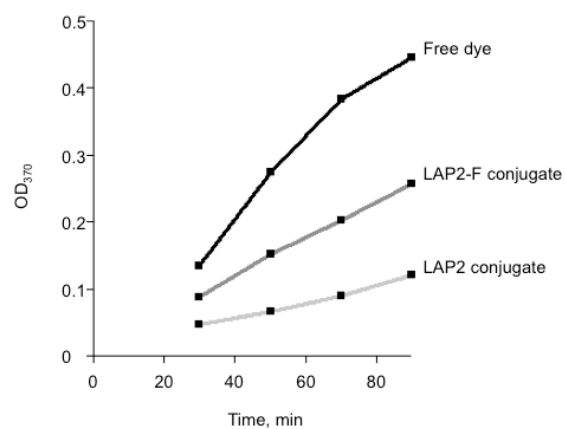
B**C**

Fig. S9. Enhancement of resorufin **2** fluorescence and photooxidation capability by a Trp→Phe mutation in LAP. **(A)** Full sequences of LAP, LAP-F, and partial sequence of E2p (a 9 kDa natural lipoyl acceptor domain of LplA) (5) in the vicinity of the acceptor lysine residue (underlined). The tryptophan residue in LAP is shown in bold face. **(B)** Resorufin **2** conjugates to LAP, LAP-F, and E2p were purified and the fluorescence emission measured, normalized against resorufin absorption at $\lambda_{\text{max,ab}}$. Emission of conjugates as a percentage of free dye is shown. Assuming that resorufin extinction coefficient does not change upon ligation to the peptide, we estimate a reduced resorufin fluorescence quantum yield (Φ_f) of 0.19 for the LAP conjugate and 0.49 for the LAP-F conjugate, compared to 0.75 for the free dye (6). **(C)** 5 μM resorufin **2** free dye or peptide conjugate was mixed with 0.5 mg/mL diaminobenzidine and irradiated. Absorbance at 370 nm is measured over time and indicates the extent of diaminobenzidine polymerization.

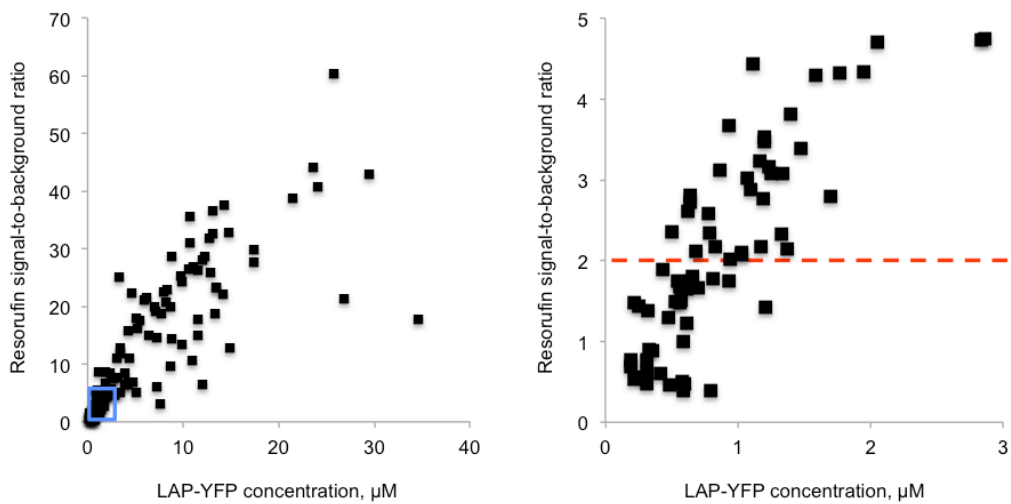


Fig. S10. Determination of resorufin labeling sensitivity. *Left:* HEK cells expressing nuclear LAP-YFP and resorufin ligase were labeled with resorufin 2-AM₂ with the 30 min. protocol in Fig. S6 then imaged live under an epifluorescence microscope. LAP-YFP concentrations in individual cells were estimated using the “wedge method” (7) (described in Supporting Methods) and plotted on the horizontal axis. Resorufin imaging signal-to-background ratios (defined in Supporting Methods) corresponding to these cells were calculated and plotted on the vertical axis. *Right:* a zoom in of the blue boxed region of the graph on the left. The red dashed line denotes a signal-to-noise ratio of 2. 150 cells from 6 fields of view were used for this plot.

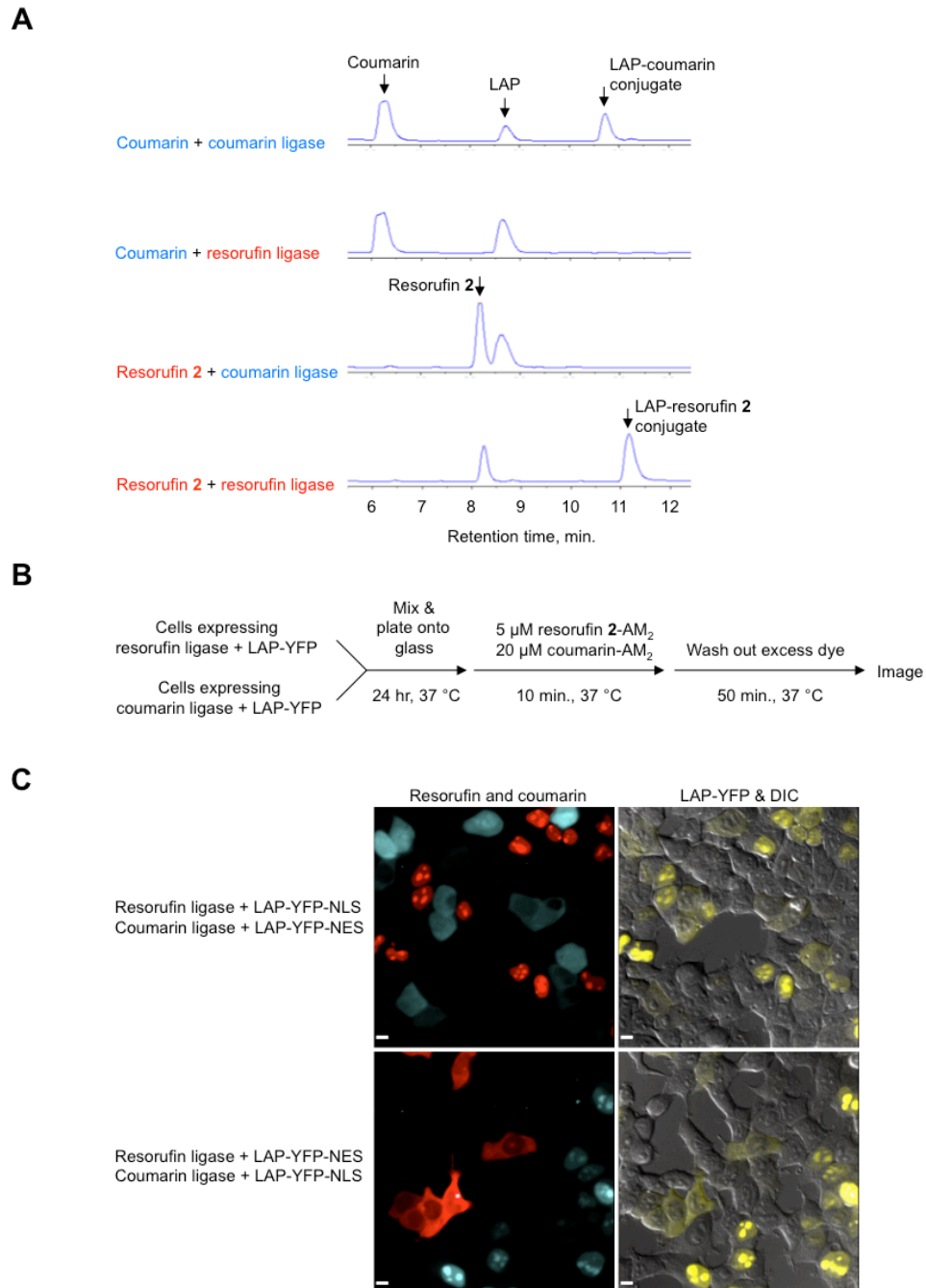


Fig. S11. Orthogonal substrate binding by coumarin and resorufin ligases. **(A)** HPLC analysis of substrate specificity. Products were not observed when resorufin 2 was combined with coumarin ligase, or coumarin was combined with resorufin ligase. **(B)** Labeling scheme for two-color resorufin and coumarin labeling in cell mixtures. **(C)** Imaging results of HEK cells treated with protocol from **(B)**. Resorufin and coumarin fluorescence were observed in neighboring cells, but never in the same cell. To further facilitate distinction, nuclear-targeted (NLS) or nuclear-excluded (NES) versions of LAP-YFP were used, as indicated. Scale bars, 10 μm .

Data set	Apo ligase	Ligase with resorufin sulfamoyladenosine bound
Beamline	APS, 24-ID-C	APS, 24-ID-C
Wavelength (Å)	0.9795	0.9795
Resolution range (Å)	44.98 – 2.151 (2.23 – 2.15)	49.98 – 3.50 (3.63 – 3.50)
Space group	<i>P</i> 2 ₁ 2 ₁ 2 ₁	<i>P</i> 2 ₁
Unit cell: a, b, c (Å)	79.1 90.0 108.9	91.4 100.0 107.3
α, β, γ (°)	90 90 90	90 105.8 90
Total reflections	230379	60149
Unique reflections	42531 (4040)	21542 (1468)
Multiplicity	5.4 (4.6)	2.8 (1.9)
Completeness (%)	99.1 (95.5)	92.0 (66.7)
Mean I/σ(I)	13.0 (2.3)	7.8 (2.3)
Wilson B-factor (Å ²)	38.9	68.2
R-sym	0.067 (0.541)	0.139 (0.265)
R-factor	0.226	0.214
R-free	0.277	0.252
Number of chains	2	4
Number of atoms	5448	10776
Protein	5136	10588
Resorufin-AMP	82 (rest disordered)	
Resorufin sulfamoyladenosine		188
Solvent	174	
Protein residues	650	1360
RMS(bonds)	0.007	0.008
RMS(angles)	0.90	0.70
Ramachandran favored (%)	94	95
Ramachandran outliers (%)	0.78	0.3
Average B-factor (Å ²)		
Protein	45.2	49.0
Resorufin-AMP	39.6	
Resorufin sulfamoyladenosine		54.4
Solvent	43.40	

Table S1. X-ray diffraction of resorufin ligase structures. Statistics for the highest resolution shell are shown in parentheses. R-factor = $\Sigma(|F_{\text{obs}}| - k|F_{\text{calc}}|) / \Sigma|F_{\text{obs}}|$ and R-free is the R value for a test set of reflections consisting of 5% of the diffraction data not used in refinement.

Supporting Methods

Chemical sources and product characterization for synthesis

Unless otherwise stated, all reagents and solvents for chemical synthesis were purchased from commercial sources (Sigma-Aldrich, Acros Organics, Alfa Aesar, or TCI America) and used without further purification. Reactions were monitored using analytical thin-layer chromatography (0.25 mm silica gel 60 F₂₅₄ plates, EMD Biochemicals). Desired products were purified by either flash column chromatography with normal phase silica gel or by HPLC (Varian Prostar with a Varian Microsorb 300-5 C₁₈ Dynamax column). Products were characterized by ¹H and ¹³C NMR (Bruker Avance 400) and by electro-spray ionization mass spectrometry (Applied Biosystems 200 QTRAP). Precipitant chemicals for protein crystallization were purchased from Hampton or Sigma-Aldrich.

Genetic constructs

Constructs used in this study are summarized below with important features listed.

Plasmids for *E. coli* expression:

Name	Features	Notes
LplA in pYFJ16 for enzymatic characterization and cell surface labeling	His ₆ -LplA	Mutations at E20, F147, and H149 generated by QuikChange. E20 and W37 mutants for Fig. S1 were previously reported (8).
^{AAAG} LplA in pYFJ16 for crystallization	His ₆ -TEV- ^{AAAG} LplA	TEV (TEV protease cleavage sequence) = ENLYFQ//G.
^{L17G/R70S/H149S} LplA in pET21a	His ₆ - ^{L17G/R70S/H149S} LplA	

Plasmids for mammalian cell expression:

Name	Features	Notes
^{AAAG} LplA in pcDNA3	His ₆ -FLAG- ^{AAAG} LplA	FLAG = DYKDDDDK.
GFP- ^{AAAG} LplA in pcDNA3	GFP-FLAG- ^{AAAG} LplA	FLAG = DYKDDDDK.
^{W37V} LplA in pcDNA3	His ₆ -FLAG- ^{W37V} LplA	Previously reported (2). FLAG = DYKDDDDK.
LAP-BFP in pcDNA3	His ₆ -LAP-BFP	Previously reported (9). LAP = GFEIDK <u>V</u> WYDLDA. Lys→Ala mutation in LAP prepared by QuikChange.
LAP-YFP in pcDNA3	His ₆ -LAP-YFP	Previously reported (2). LAP = GFEIDK <u>V</u> WYDLDA. Lys→Ala mutation in LAP prepared by QuikChange.
LAP-YFP-NLS in pcDNA3	His ₆ -LAP-YFP-NLS	Nuclear localized LAP-YFP. Previously reported (2). LAP = GFEIDK <u>V</u> WYDLDA. NLS = nuclear localization signal.
LAP-YFP-NES in pcDNA3	His ₆ -LAP-YFP-NES	Nuclear excluded LAP-YFP. Previously reported (2). LAP = GFEIDK <u>V</u> WYDLDA.
LAP-YFP-CaaX in pcDNA3	His ₆ -LAP-YFP-CaaX	Membrane-anchored LAP-YFP. Previously reported (2).

		LAP = GFEID <u>K</u> VWYDLDA. CaaX = prenylation motif.
LAP-LDL receptor in pcDNA4TO	SS-LAP-HA-LDL receptor	Previously reported (10). SS = signal sequence. LAP = GFEID <u>K</u> VWHDFPA. HA = YPYDVDPYA.
LAP-β-actin in Clontech vector	HA-LAP-β-actin	Previously reported (2). HA = YPYDVDPYA. LAP = GFEID <u>K</u> VWYDLDA.
Vimentin-LAP in Clontech vector	Vimentin-LAP-C-myc	Previously reported (2). C-myc = EQKLISEEDL. LAP = GFEID <u>K</u> VWYDLDA.
LAP-MAP2 in Clontech vector	HA-LAP-MAP2	Previously reported (2). HA = YPYDVDPYA. LAP = GFEID <u>K</u> VWYDLDA.
HaloTag-β-actin in Clontech vector	HA-HaloTag-β-actin	HA = YPYDVDPYA.

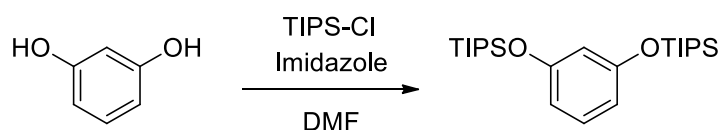
Other notes:

^{AAG}LpIA = ^{E20A/F147A/H149G}LpIA (resorufin ligase).

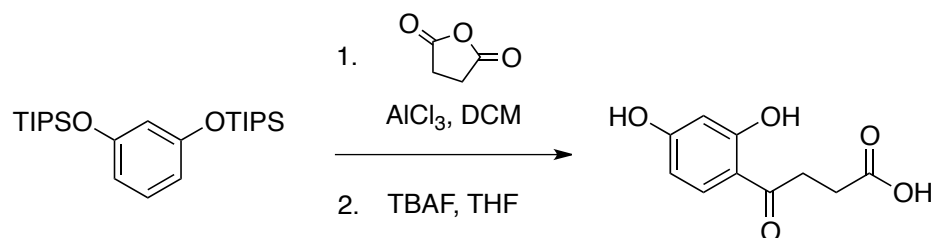
^{L17G/R70S/H149S}LpIA is top-scoring Rosetta design (16_92).

Lysine residue in LAP for resorufin conjugation is underlined.

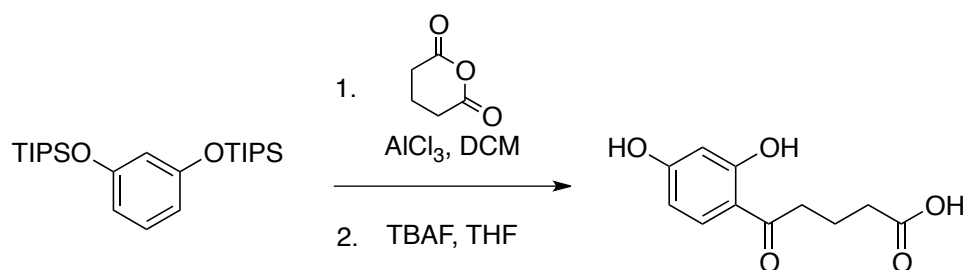
Synthesis of resorufin substrates (Fig. 1B and Fig. S4B)



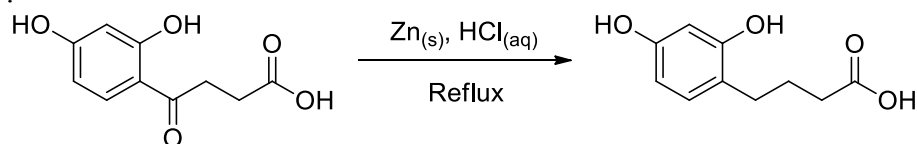
A dry round-bottom flask equipped with a magnetic stir bar was charged with 2 g resorcinol (18.2 mmol) and 50 mL anhydrous *N,N*-dimethylformamide under a nitrogen atmosphere. 8.55 mL triisopropylsilyl chloride (40.0 mmol) and 2.47 g imidazole (36.3 mmol) were then added to the flask and the mixture stirred at room temperature for 24 hr. The reaction mixture was diluted with 500 mL water and the organics extracted twice into ethyl acetate. The combined ethyl acetate solution was washed with 50 mL of 1 M sodium bicarbonate solution, followed by 50 mL of brine, then dried with sodium sulfate. The volatiles were removed via rotary evaporation to give a clear, colorless oil. Purification by normal-phase column chromatography (100% hexanes) yielded 6.5 g of the desired product as a colorless liquid (yield 85%). ¹H-NMR (400 MHz, acetone-*D*₆): 7.11 (t, 1H, *J* = 8.1), 6.53 (dd, 2H, *J* = 8.2, 2.3), 6.47 (t, 1H, *J* = 2.3), 1.33 – 1.20 (m, 6H), 1.11 (m, 36H). ¹³C-NMR (400 MHz, acetone-*D*₆): 158.0, 130.7, 114.0, 112.5, 18.3, 13.4.



A dry round-bottom flask equipped with a magnetic stir bar was charged with 800 mg 1,3-bis((triisopropylsilyloxy)benzene (1.89 mmol) and 16 mL anhydrous dichloromethane under a nitrogen atmosphere. 248 mg succinic anhydride (2.48 mmol) and 256 mg aluminum chloride (1.92 mmol) were then added to the flask and the mixture stirred at room temperature for 9 hr. The volatiles of the reaction mixture were removed via rotary evaporation, and the resulting solids partitioned between 200 mL water and 200 mL ethyl acetate. The ethyl acetate layer was dried with sodium sulfate and the solvent removed under vacuum to give a clear, yellow oil. This oil was dissolved in 20 mL tetrahydrofuran and reacted with 2 mL of 1 M tetra-*n*-butylammonium fluoride in tetrahydrofuran for 5 min. at room temperature. The volatiles were removed via rotary evaporation, and the resulting green wax extracted with a 1:1 mixture of ethyl acetate: 0.1 M HCl_(aq). The ethyl acetate layer was dried with sodium sulfate and the solvent removed via rotary evaporation to give a green oil. Purification by normal-phase column chromatography (1:9 methanol:dichloromethane) yielded 330 mg of the desired product as a yellow oil (overall yield 83%). ¹H-NMR (400 MHz, acetone-D₆): 12.58 (s, 1H), 10.1 (bs, 1H), 7.87 (d, 1H, *J* = 8.8), 6.46 (dd, 2H, *J* = 8.8, 2.4), 6.32 (d, 2H, *J* = 2.4), 3.31 (t, 2H, *J* = 6.3), 2.71 (t, 2H, *J* = 6.5). ESI-MS(-) calculated for [M-H]⁻: 209.05; found 209.0.

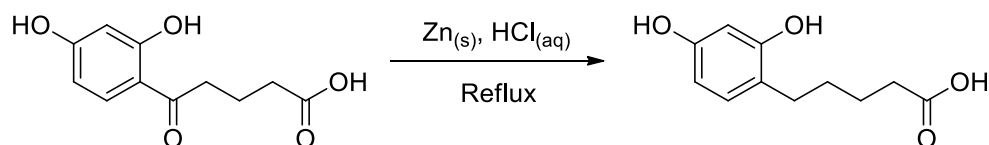


Reaction was set up according to above, with 500 mg 1,3-bis((triisopropylsilyloxy)benzene (1.18 mmol), 180 mg glutaric anhydride (1.58 mmol), 170 mg aluminum chloride (1.27 mmol) in 40 mL anhydrous dichloromethane. Deprotection of silyl groups by tetra-*n*-butylammonium fluoride and subsequent extraction were carried out as above. Purification by normal-phase column chromatography (1:9 methanol:dichloromethane) yielded 210 mg of desired product as a yellow oil (yield 79%). ¹H-NMR (400 MHz, acetone-D₆): 7.82 (d, 1H, *J* = 8.8), 6.46 (dd, 1H, *J* = 8.8, 2.4), 6.35 (d, 1H, *J* = 2.4), 3.06 (t, 2H, *J* = 7.6), 2.44 (t, 2H, *J* = 7.2), 1.96 (m, 2H). ¹³C-NMR (400 MHz, CDCl₃): 203.62, 178.20, 164.87, 163.22, 131.48, 113.86, 112.09, 107.91, 36.60, 32.96, 19.24. ESI-MS(-) calculated for [M-H]⁻: 223.07; found 223.20.

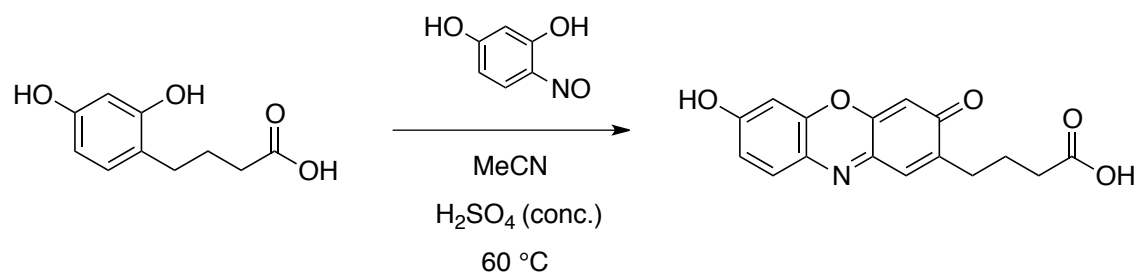


A round-bottom flask equipped with a magnetic stir bar was charged with 250 mg 4-(2,4-dihydroxyphenyl)-4-oxobutanoic acid (1.90 mmol), 20 mL H₂O, 20 mL concentrated hydrochloric acid, and 870 mg zinc powder (13.3 mmol). The reaction was heated under reflux

with stirring for 16 hr, then cooled to room temperature, diluted with 100 mL water and adjusted to pH 2 with solid sodium bicarbonate. The aqueous mixture was extracted three times with 50 mL ethyl acetate. The combined ethyl acetate layers were dried with sodium sulfate, and the volatiles removed under rotary evaporation to give a brown oil. Purification by normal-phase column chromatography (100% ethyl acetate) yielded 174 mg of the desired product as a white solid (yield 75%). ¹H-NMR (400 MHz, acetone-D₆): 8.05 (bs, 1H), 6.87 (d, 1H, *J* = 8.1), 6.38 (d, 1H, *J* = 2.4), 6.27 (dd, 1H, *J* = 8.1, 2.4), 2.54 (t, 2H, *J* = 7.7), 2.30 (t, 2H, *J* = 7.5), 1.84 (m, 2H). ¹³C-NMR (400 MHz, acetone-D₆): 175.19, 173.97, 157.59, 156.80, 131.44, 119.75, 107.32, 103.46, 33.77, 26.32. ESI-MS(-) calculated for [M-H]⁻: 195.07; found 195.0.

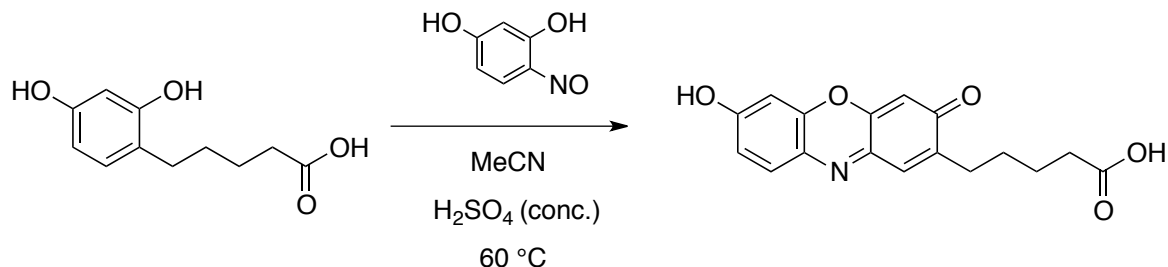


Reaction was set up according to above, with 83 mg 5-(2,4-dihydroxyphenyl)-4-oxopentanoic acid (370 μmol), 10 mL H₂O, 10 mL concentrated hydrochloric acid, and 72 mg zinc powder (1.10 mmol). After refluxing for 18 hr, the mixture was basified and extracted as above. Purification by normal-phase column chromatography (100% ethyl acetate) yielded 25 mg of the desired product as a white solid (yield 32%). ¹H-NMR (400 MHz, acetone-D₆): 8.48 (bs, 2H), 6.87 (d, 1H, *J* = 8.0), 6.36 (d, 1H, *J* = 2.8), 6.26 (dd, 1H, *J* = 8.4, 2.4), 2.53 (t, 2H, *J* = 7.2), 2.31 (t, 2H, *J* = 7.2), 1.67 – 1.55 (m, 4H). ¹³C-NMR (400 MHz, acetone-D₆): 175.38, 157.27, 156.61, 131.26, 120.40, 107.32, 103.41, 34.27, 30.56, 29.79, 25.46. ESI-MS(-) calculated for [M-H]⁻: 209.09; found 209.16.

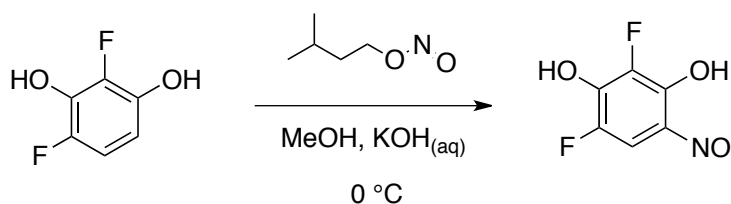


A glass vial equipped with a magnetic stir bar was charged with 10 mg 4-(2,4-dihydroxyphenyl)butanoic acid (51 μmol), 2.0 mL acetonitrile, and 0.25 mL concentrated sulfuric acid. 7.0 mg of 4-nitrosoresorcinol (Chemos, 50.3 μmol) was added to the mixture, and the reaction stirred at 60 °C for 4 hr. The mixture was then diluted with 30 mL water and extracted three times with 20 mL ethyl acetate. The combined ethyl acetate layers were dried with sodium sulfate, and the volatiles removed under rotary evaporation to give a dark purple solid. The desired product was purified by preparatory HPLC (Varian ProStar) on a C₁₈ column (Agilent Dynamax Microsorb 300-5) using a 0% to 70% acetonitrile linear gradient over 20 min. The aqueous solution was freeze-dried to give 1.2 mg of dark purple solid (yield 8%). ¹H-NMR

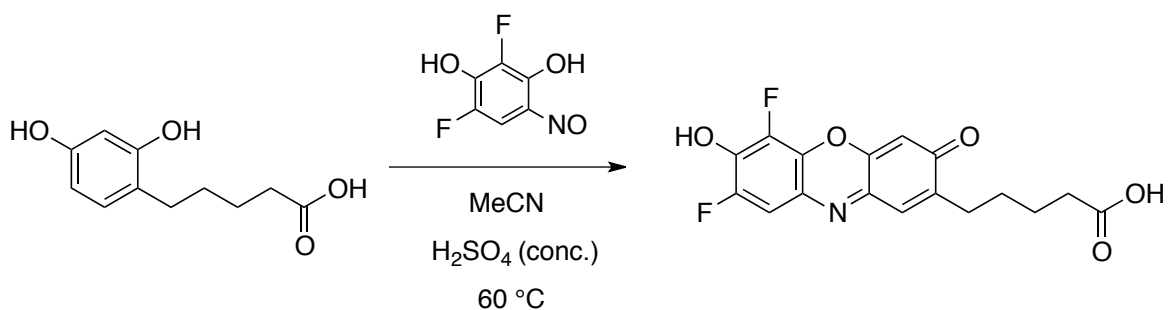
(400 MHz, D₂O): 7.36 (d, 1H), 7.16 (d, 1H), 6.67 (dd, 1H), 6.38 (s, 1H), 6.29 (s, 1H), 2.41 (t, 2H), 2.20 (t, 2H), 1.80 – 1.70 (m, 2H). ESI-MS(+) calculated for [M+H]⁺: 300.08; found 300.2.



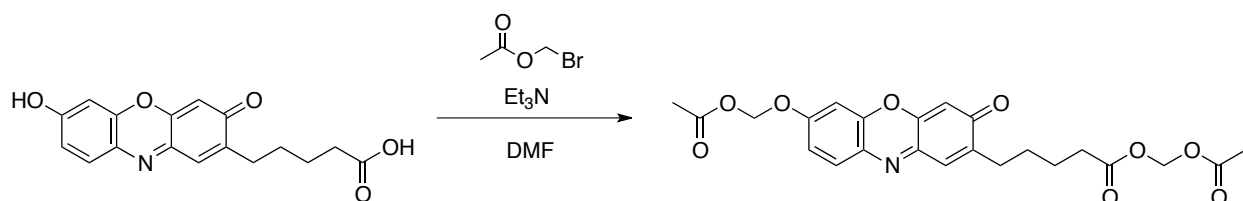
Reaction was set up according to above, with 40 mg 5-(2,4-dihydroxyphenyl)pentanoic acid (190 μ mol), 28 mg 4-nitrosoresorcinol (205 μ mol), 2.0 mL acetonitrile, and 0.25 mL concentrated sulfuric acid. After heating at 60 °C for 4 hr, the mixture was extracted as above, then dried to give a dark purple solid. The solids were dissolved in H₂O containing 0.5% (v/v) ammonium hydroxide and loaded onto a Sep-Pak Vac 12cc 2g C₁₈ cartridge (Waters). Purification of the desired product was carried out by successive 5-mL elutions of 0, 10, 20, 30, and 40% acetonitrile in H₂O (v/v). The aqueous solution was freeze-dried to give 4.6 mg of dark purple solid (yield 8%). ¹H-NMR (400 MHz, D₂O doped with NH₄OH): 7.44 (d, 1H, *J* = 9.2), 7.24 (s, 1H), 6.74 (dd, 1H, *J* = 9.2, 2.4), 6.45 (d, 1H, *J* = 2.4), 2.49 (t, 2H, *J* = 7.6), 2.25 (t, 2H, *J* = 7.4), 1.66 – 1.56 (m, 4H). ¹³C-NMR (400 MHz, D₂O doped with NH₄OH and acetone-D₆): 184.19, 183.93, 180.70, 150.14, 149.68, 141.22, 133.67, 132.05, 129.52, 129.34, 124.60, 103.87, 103.83, 38.02, 29.62, 28.01, 26.32. ESI-MS(+) calculated for [M+H]⁺: 314.10; found 314.2.



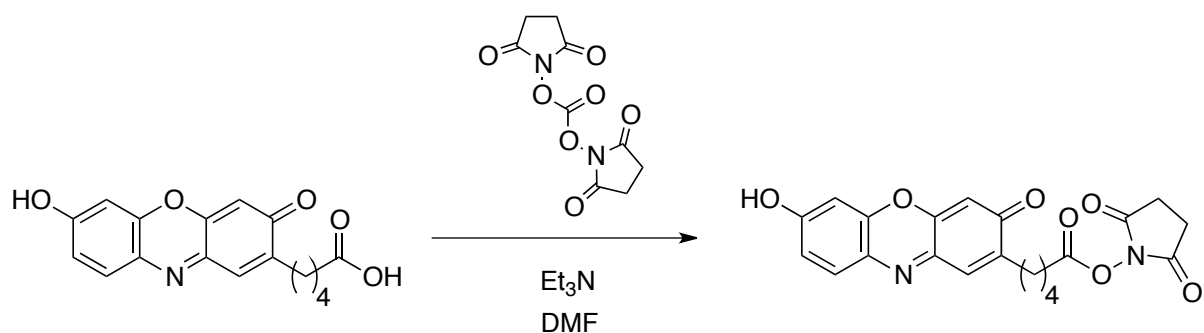
A glass vial equipped with a magnetic stir bar was charged with 100 mg 2,4-difluoro-6-hydroxyresorcinol (684 μ mol), 3.4 mL methanol, and 86 mg potassium hydroxide (1.54 mmol) dissolved in 300 μ L H₂O. The mixture was cooled to 0 °C in an ice-water bath. 160 μ L isopentyl nitrite (1.20 mmol) was added to the reaction in 5 portions over 30 min. while stirring at 0 °C. The reaction mixture was then removed from the ice bath and naturally warmed to room temperature and stirred for a further 24 hr. After this time, the mixture was diluted with 40 mL water and acidified with concentrated hydrochloric acid dropwise until pH 2, at which point a light brown precipitate formed. This precipitate was collected by centrifugation and washed twice with cold 0.1 M hydrochloric acid, then dried under vacuum to give 82 mg of the desired product as a tan solid (yield 68%). ¹H-NMR (400 MHz, D₂O): 6.81 (d, 1H, *J* = 10.8). ESI-MS(-) calculated for [M-H]⁻: 174.01; found 174.1.



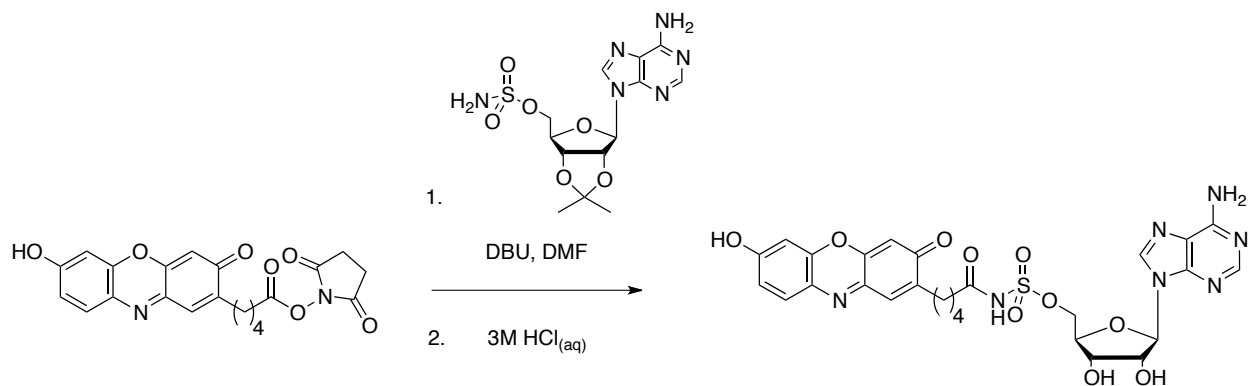
A glass vial equipped with a magnetic stir bar was charged with 20 mg 5-(2,4-dihydroxyphenyl)pentanoic acid (95.2 μmol), 2.0 mL acetonitrile, and 0.25 mL concentrated sulfuric acid. 17 mg of 2,4-difluoro-6-nitrosoresorcinol (97.0 μmol) was added to the mixture, and the reaction stirred at 60 $^\circ\text{C}$ for 4 hours. The mixture was then diluted with 20 mL water and extracted three times with 20 mL ethyl acetate. The combined ethyl acetate layers were dried with sodium sulfate, and the volatiles removed under rotary evaporation to give a dark purple solid. The desired product was purified as above for resorufin **2**. The aqueous solution was freeze-dried to give 1.7 mg of dark purple solid (yield 5%). $^1\text{H-NMR}$ (400 MHz, D_2O): 7.13 (s, 1H), 7.10 (d, 1H, $J = 10.9$), 6.37 (s, 1H), 2.45 (t, 2H, $J = 7.6$), 2.28 (t, 2H, $J = 7.5$), 1.67 – 1.53 (m, 4H). ESI-MS(+) calculated for $[\text{M}+\text{H}]^+$: 350.08; found 350.1.



A dry round-bottom flask equipped with a magnetic stir bar was charged with 10 mg resorufin **2** (32 μmol), 1.5 mL anhydrous DMF, and 80 μL anhydrous triethylamine under a nitrogen atmosphere. 25 μL bromomethyl acetate (255 μmol) was added over 3 min. via a dry syringe. The reaction mixture was stirred at room temperature for 6 hours, then diluted with 30 mL phosphate buffered saline, pH 7.4, and extracted three times with 15 mL ethyl acetate each. The combined ethyl acetate extracts were dried with sodium sulfate and the volatiles removed under rotary evaporation to give a brown oil. The desired *trans*-protected product was purified by preparatory HPLC using a Varian Microsorb 300-5 C_{18} Dynamax column under a 20% to 80% acetonitrile linear gradient (flow rate = 10 mL/min.) over 40 min. and was eluted at 22 min. The *cis*-protected isomer eluted at 23 min. This separation was only observed when less than 3 mg dry mixture was loaded onto the column, dissolved in 80% acetonitrile. The *trans*:*cis* product ratio was typically $\sim 1:10$. After removal of acetonitrile under rotary evaporation, the aqueous solution was freeze-dried to give ~ 1 mg orange-colored solid. The yield was difficult to measure accurately. $^1\text{H-NMR}$ (400 MHz, acetone- D_6): 7.65 (s, 1H), 7.47 (d, 1H), 7.23 (s, 1H), 6.77 (dd, 1H), 6.20 (d, 1H), 5.99 (s, 2H), 5.72 (s, 2H), 2.72 (t, 2H), 2.42 (t, 2H), 1.72 – 1.63 (m, 4H). ESI-MS(+) calculated for $[\text{M}+\text{H}]^+$: 458.14; found 458.3.



A glass vial equipped with a magnetic stir bar was charged with 5 mg resorufin **2** (16 μmol), 6 mg *N,N'*-disuccinimidyl carbonate (24 μmol), and 5 μL triethylamine (36 μmol) dissolved in 1 mL *N,N*-dimethylformamide. The mixture was stirred at room temperature for 6 hr. After this time, the mixture was diluted with 40 mL phosphate buffered saline, pH 7.4, then extracted twice with ethyl acetate. The combined organic washes were dried with sodium sulfate and the volatiles removed via rotary evaporation. Purification by normal-phase column chromatography (100% ethyl acetate) yielded 5 mg of the desired product as a dark red solid (yield 76%). $^1\text{H-NMR}$ (400 MHz, acetone- D_6): 7.65 (d, 1H, $J = 8.8$), 7.33 (t, 1H, $J = 1.1$), 6.94 (dd, 1H, $J = 8.8$, 2.5), 6.90 (d, 1H, $J = 2.5$), 6.22 (s, 1H), 2.87 (s, 4H), 2.72 (t, 2H, $J = 7.2$), 2.62 (t, 2H, $J = 6.7$), 1.85 – 1.70 (m, 4H). ESI-MS(-) calculated for $[\text{M-H}]^-$: 409.38; found 409.2.



A glass vial equipped with a magnetic stir bar was charged with 5 mg resorufin **2** succinimidyl ester (12 μmol), 6 mg 2',3'-isopropylidene sulfamoyl adenosine (Alchem Laboratories, 16 μmol), and 5 μL 1,8-diazabicycloundec-7-ene (33 μmol) dissolved in 1 mL *N,N*-dimethylformamide. The mixture was stirred at room temperature for 16 hr. After this time, the mixture was diluted with 40 mL H_2O then extracted twice with ethyl acetate. The combined organic washes were dried with sodium sulfate and the volatiles removed via rotary evaporation. The resulting purple solid was stirred in 1 mL 3 M $\text{HCl}_{(\text{aq})}$ for 6 hr. The aqueous solvent was then removed by rotary evaporation and the residual orange solid dissolved in 1 mL H_2O containing 1% ammonium hydroxide to give a dark purple solution. This solution was loaded onto a Sep-Pak Vac 12cc 2g C_{18} cartridge (Waters). Purification of the desired product was carried out by successive 5-mL elutions of 0, 10, 20, and 30% acetonitrile in H_2O (v/v). The aqueous solution was freeze-dried to

give 6 mg of dark purple solid (overall yield 78%). ¹H-NMR (400 MHz, D₂O): 7.98 (s, 1H), 7.62 (s, 1H), 7.32 (d, 2H, *J* = 9.2), 6.77 (dd, 1H, *J* = 9.1, 2.44), 6.75 (s, 1H), 6.43 (d, 1H, *J* = 2.4), 6.07 (s, 1H), 5.77 (d, 1H, *J* = 5.5), 4.42 – 4.36 (m, 5H), 2.40 – 2.30 (m, 4 H), 1.74 (m, 2H), 1.45 (m, 2H). ESI-MS(-) calculated for [M-H]⁻: 640.15; found 640.3.

Computational redesign of LplA to accommodate resorufin 2-AMP (Fig. 2 and Fig. S2)

All calculations were carried out with Rosetta revision 36000 and energies are in Rosetta Energy Units using the enzdes.wts weight set.

Step 1 Generation of resorufin 2-AMP conformers

500 conformers of resorufin 2-AMP were generated in Omega by diversifying the 5-carbon linker of resorufin 2-AMP. The atomic coordinates for the adenosine and the phosphate moieties were taken from those of lipoyl-AMP in the lipoyl-AMP-bound crystal structure of LplA (PDB ID 3A7R(1)) and held constant. The conformational diversity of the resorufin 2-AMP model was thus restricted to the resorufin moiety.

Step 2 Iterative design of LplA sequences through cycles of rotamer substitution and gradient-based energy minimization

A set of 16 resorufin 2-AMP rotamers that do not clash with the LplA backbone when superimposed onto the AMP moiety in 3A7R were selected from the 500 member conformer library. Combining each of these non-clashing rotamers with the LplA coordinates in 3A7R led to 16 starting structures for the design process.

For each starting structure, at the beginning of each trial, resorufin 2-AMP was randomly perturbed by a small shift or rotation of the resorufin 2 center of mass. All LplA side-chains whose C_α atom is < 6 Å away from any non-H atom of resorufin 2-AMP were allowed to mutate to any other amino acid or sample other conformations, except that residues directly contacting adenosine, phosphate or alkyl chain of the lipoyl (residues 75, 76, 77, 78, 79, 83, 121, 133, 135, 136, 137, 151, 153, 161, 165, 179, 180, 181, 182, 184) were always fixed according to wild-type LplA, to preserve basic catalytic activity and known mutation-sensitive sites. Additionally, all side-chains < 8 Å away were allowed to mutate or change conformation if their C_α→C_β vector are pointing in the direction of lipoyl-AMP. Allowed conformations of amino acid side chains were taken from the library created by Dunbrack and co-workers (11). A flat penalty of 7 Rosetta energy units in LplA global energy was imposed on any mutations in order to favor native sequences and therefore reduce chances of protein mis-folding or destabilization *in vitro*; the resulting designs therefore have few mutations and sequence diversity in designs is relatively low.

1600 independent Monte Carlo simulations were carried out, where sampling occurred in both sequence and structure space with only very small (up to 0.1 Å) motions allowed in the backbone during minimization steps. In each run a “repack” of side chain and resorufin 2 conformers was carried out followed by a gradient based minimization, and the cycle of repacking/minimization was repeated twice. During a repacking, side chain and resorufin conformers were allowed to change, and residues were allowed to mutate. Each change was accepted or rejected with a

Metropolis Monte Carlo criterion (decreasing energy is always accepted, increasing energy is accepted with exponentially decreasing probability; steps with a big increase in energy are extremely improbable). The probability of accepting moves with increased energy was gradually decreased during the simulation, a protocol known as “simulated annealing” which can help find optimal sequences.

At this stage there were roughly 40,000 allowed rotamers (counting over all rotamers over all allowed identities at each of the roughly 24 designable positions), and a typical run would involve $> 10^6$ individual packer steps. In each packer step a position was selected at random and then a new rotamer or amino acid identity was selected. For example, in a single step we might find that position 13 is an alanine; we then randomly choose to change it to a valine with a common valine conformation; we then recalculate the energy of LplA and find it has decreased by 1 Rosetta energy unit, so we accept the pack move. This was repeated millions of times, where the number of repeats scales with the number of allowed rotamers. Minimization of resorufin 2-AMP rigid body location, side chain and backbone degrees of freedom was then carried out and the cycle of repack/minimization was repeated. We performed this cycle twice so the backbone was allowed to adjust to accommodate any changes from the first repack cycle.

The crucial aspects of this procedure are that sequence and structure space were optimized simultaneously and that the entire sequence space was implicitly sampled over all designable residues, so the number of sequences considered here (for a very limited backbone conformational space) is 20^{24} .

This algorithm for design on a fixed backbone was first developed and shown to be effective for the design of entire globular protein folds (12). The details of the algorithm, such as the number of cycles, the method of calculating energies for new conformations, and the simulated annealing protocol, have been optimized in detail by attempting to reproduce the sequences of natural proteins given only their backbone coordinates (13).

Computational prediction of coumarin ligase structure with coumarin-AMP bound (Fig. 2A)

We used the Rosetta fixed backbone ligand docking application (14). First, 500 conformers of the coumarin-AMP were generated in Omega, keeping the AMP fixed, as for resorufin 2. Then 5000 independent docking runs were carried out so that the best positions and conformation of the coumarin-AMP could be identified. In each run coumarin-AMP was first perturbed by a small random distance, and then six cycles of a random move followed by repacking with minimization were carried out, using the repack protocol described above. The difference here is that no residue identities were allowed to change – a leucine is always a leucine – but rotameric states were allowed to change. The other difference between this protocol and the design protocol described above is that a random move of the coumarin-AMP was applied before each new cycle, to introduce more sampling of rotation and placement degrees of freedom. After each cycle the new structure was only accepted if the energy decreased, or, if the energy increased, it was accepted with an exponentially decreasing probability of energy. The best structure by Rosetta energy arising from this set of simulations is shown as the structural prediction for the enzyme•coumarin-AMP complex.

Determination of the crystal structure of “apo” resorufin ligase (Fig. S4 and Table S1)

For the “apo” structure, crystallization was carried out in a hanging drop vapor diffusion setup, using 1 μ L of 5.5 mg/mL resorufin ligase containing 500 μ M resorufin 2, 1 mM ATP, 1 mM Mg(OAc)₂, and 1 mM dithiothreitol mixed with 1 μ L of precipitant solution (50 mM sodium cacodylate, pH 6.0, 50 mM calcium chloride, 300 mM potassium chloride, 10% PEG 3,350). Drops were incubated at 4 °C in the dark, and red colored crystalline rods appeared after ~5 days. Crystals were looped and washed through a cryoprotection solution of 50% precipitant solution, 30% LpIA buffer, and 20% ethylene glycol. Crystals were then cryocooled by direct submersion into liquid nitrogen.

Diffraction data was collected at 100 K using sequential 1° oscillations at beamline 24 ID-C of the Advanced Photon Source (APS) in Argonne, Il and processed using HKL-2000 (15). The “apo” resorufin ligase structure was solved by molecular replacement in Phaser(16) (Z-score of 57.3) using a 2.0 Å high resolution cutoff. The structure of apo wild-type LpIA (PDB 1X2G (4)) was used as the search model, following removal of waters and ligands. Two molecules of the ligase were found in the asymmetric unit. Model building was carried out in COOT (17), followed by refinement in PHENIX (18), without the use of noncrystallographic symmetry restraints or sigma cutoffs. Existing CCP4 ligand parameter files were modified using Sketcher to generate geometry restraint files for all ligands. Difference electron density maps were used to verify the E20A, F147A, and H149G mutation. Iterative rounds of model building and refinement were carried out until R-factors converged to the final values shown in Table S1. Composite omit maps were used to validate the structure.

The final model shows the apo conformation of the ligase (see Fig. S4), indicating that co-crystallization with resorufin and ATP was unable to stabilize the substrate-bound conformer long enough for crystallization, at least under these conditions. Electron density for resorufin (without AMP) is present, but not in the active site. This density in the cleft between the *N*- and *C*-terminal domains is unlikely to be catalytically relevant. The surreptitious binding of lipoic acid has also been observed in the wild-type structure (4). For these reasons, we refer to this resorufin ligase as “apo” even though it was crystallized in the presence of substrates.

Purification of LAP-resorufin 2 conjugate and measurement of fluorescence excitation/emission spectra (Fig. S3C)

To generate the conjugate, a ligation mixture were assembled with 2 μ M resorufin ligase, 400 μ M LAP (GFEIDK \underline{V} WYDLDA), 500 μ M resorufin 2, 2 mM ATP, and 5 mM Mg(OAc)₂ in DPBS containing 10% (v/v) glycerol, then reacted for 4 hours at 30 °C. The LAP-resorufin 2 conjugate was purified by HPLC (Varian Prostar) using a C₁₈ column (Microsorb-MV 300-5), under the same solvent gradient as for enzyme activity assays. The eluate was freeze-dried to give a yellow powder. To measure the excitation/emission spectra, 20 μ M resorufin 2 or LAP-resorufin 2 conjugates in Dulbecco’s phosphate buffered saline, pH 7.4, was placed in an opaque, flat-bottom 96-well plate (Greiner Bio One) and analyzed by a fluorescence microplate reader (Tecan). Excitation scans were performed at 1 nm steps and detected constantly at 615 nm. Emission scans were performed at 1 nm steps and excited constantly at 550 nm.

Measurement of Michaelis-Menten kinetic parameters for *in vitro* resorufin ligation (Fig. S3D-E)

Reaction mixtures were assembled with 500 nM resorufin ligase, 200 μ M LAP (GFEIDK \underline{V} WYDLDA), 5 mM Mg(OAc)₂, and 10 – 200 μ M resorufin 2 in DPBS containing

10% (v/v) glycerol and maintained at 30 °C. Reactions were initiated with the addition of 2 mM ATP. After 2, 4, 6, and 8 min., 50 µL of reaction mixture was drawn and quenched with a final concentration of 50 mM ethylenediaminetetraacetic acid, then analyzed by HPLC. Product conversion was measured by integrating peak areas at 210 nm detection, normalized against absorption increase of LAP due to resorufin 2 ligation. Michaelis-Menten parameters were extracted from the initial rates v. substrate plot using the Origin software.

Testing *cis* and *trans* resorufin 2-AM₂ regioisomers for washout in HEK cells and in rat neurons (Fig. S5B)

HEK cells and rat cortical neurons were cultured as in General Methods. After one rinse with serum-free MEM, cells were loaded with 5 µM of either *cis* or *trans* resorufin 2-AM₂ in the same medium for 15 min. Cells were then rinsed three times in complete growth medium and imaged after 20 min. or 1 hr.

Measurement of cellular resorufin ligation yield by a gel-shift assay (Fig. S6)

HEK cells grown in 6-well plates were transfected with 800 ng DNA/well LAP-tagged YFP and 400 ng DNA/well resorufin ligase. 24 hr after transfection cells were labeled with resorufin 2-AM₂ for 10 – 30 min. with additional 45 min. dye washout and subsequently lysed as in Fig. 3B. The lysate was centrifuged at 8000 g for 10 min. at 4 °C. The clarified lysate was loaded onto an 8% polyacrylamide gel (containing SDS) in loading buffer lacking SDS and without sample boiling (to preserve YFP fluorescence). Gel electrophoresis was carried out at 4 °C. The gel was imaged using a Fujifilm FLA-9000 image scanner with 473 nm excitation, blue long-pass filter for YFP visualization and 532 nm excitation, green long-pass filter for resorufin visualization. The same gel was then stained by Coomassie and re-imaged under white light. YFP densitometry was performed using the Multi Gauge software.

Comparing resorufin and immunofluorescence labeling of actin and vimentin (Fig. S7)

HeLa cells expressing GFP-tagged resorufin ligase and either HA-LAP-β-actin or vimentin-C-myc-LAP were transfected and labeled as in Fig. 3C, except that the resorufin 2-AM₂ labeling time was 30 min. After one rinse with DBPS, cells were fixed with 3.7% formaldehyde for 15 min. and permeabilized by cold methanol for 2 min. Cells were then blocked with 0.5% (w/v) casein in DPBS for 4 hr at room temperature. For LAP-β-actin cells, immunostaining was performed with a 1:300 dilution of rabbit anti-HA antibody (Rockland) in the same buffer for 30 min., followed by three rinses and secondary staining with 1:300 dilution of goat-anti-rabbit antibody Alexa Fluor 647 conjugate (Life Technologies) for 20 min. Cells were imaged after three final rinses with the same buffer. Vimentin-C-myc-LAP cells were immunostained under identical conditions using mouse anti-C-myc antibody (Calbiochem) and goat-anti-mouse antibody Alexa Fluor 647 conjugate (Life Technologies).

Measurement of resorufin 3 phenolic pKa (Fig. S8B)

10 µM solutions of resorufin 3 were prepared in 100 mM citrate buffers ranging from pH 3 to pH 6 and placed in a 96-well opaque-wall plate. Absorbance at 570 nm was measured using a microplate reader (Tecan) as a readout of phenolic protonation state.

Live cell surface labeling with resorufin (Fig. S8C)

HEK on glass coverslips were transfected with LAP-low density lipoprotein receptor and GFP (as a transfection marker). 18 hr later, cells were rinsed once with serum-free MEM, then treated with Tyrode's buffer containing 5 μ M resorufin ligase, 25 μ M resorufin 2 or resorufin 3, 1 mM ATP, 2 mM Mg(OAc)₂ and 0.5% (w/v) casein for 10 min. at room temperature. Cells were then rinsed three times with complete growth medium and imaged live in DPBS.

Measurement of resorufin-catalyzed diaminobenzidine polymerization (Fig. S9C)

Resorufin 2 conjugates to LAP (GFEIDK \underline{V} WYDLDA) and LAP-F (GFEIDK \underline{V} FYDLDA) were purified as in Fig. S3C. 5 μ M of the free dye or peptide conjugate was mixed with 0.5 mg/mL diaminobenzidine in DPBS, pH 7.4, and placed in plastic cuvettes, then irradiated with a 75W incandescent light bulb. 100 μ L aliquots were withdrawn at 30, 50, 70, and 90 min. and their absorbance at 370 nm measured with a NanoDrop spectrophotometer (Thermo Scientific).

Determination of resorufin labeling and mCherry tagging sensitivity (Fig. S10)

To determine resorufin labeling sensitivity, HEK cells were transfected and labeled using the 30 min. protocol in Figure S6 with the exception that cells were plated in 48-well plates and the amount of plasmid was scaled accordingly, then imaged live. To determine mCherry sensitivity, HEK cells were transfected with LAP-mCherry and imaged live after 24 hr.

The wedge method (7), requiring purified fluorescent protein standards, was used to estimate the LAP-YFP-NLS and LAP-mCherry concentrations inside cells. YFP and mCherry carrying terminal His₆ tags were overexpressed in *E. coli* at room temperature. YFP and mCherry plasmids were gifts from J. Martell and W. Wang, respectively. Cells were lysed using the B-PER reagent (Thermo Scientific) supplemented with protease inhibitor cocktail (Sigma-Aldrich) and the lysate was clarified by centrifugation at 8000 g for 10 min. Desired protein from the supernatant was purified by nickel immobilized metal affinity chromatography and subsequently dialyzed into DPBS. Chromophore absorption was measured using a NanoDrop spectrophotometer (Thermo Scientific) and converted into concentrations using published extinction coefficients (19). A wedge-shaped chamber constructed from No. 1.5 glass coverslips was filled with 20 μ M YFP or mCherry protein and imaged. Fluorescence intensities at 5 μ m chamber thickness were measured.

Imaging was carried out on a Zeiss AxioObserver epifluorescence microscope using a 20X air objective. YFP (493/16 excitation, 525/30 emission, 500 dichroic) and mCherry/resorufin (both 570/20 excitation, 605/30 emission, 585 dichroic) fluorescence were acquired for 500 ms. Imaging data was processed using SlideBook software version 5.0 (Intelligent Imaging Innovations). Circular masks within the boundaries of the cells or nuclei were drawn for 150 cells visibly expressing YFP or mCherry across 6 fields-of-view. The mean YFP/resorufin or mCherry fluorescence intensities (I) from these masks were tabulated. Instrument noise (N_{Inst}) for all fluorescence channels was measured from an image of an empty, untreated glass coverslip. Resorufin and mCherry cellular backgrounds (N_{Cells}) were measured from respective samples in cell-covered regions not visibly expressing the fluorescent protein. The tabulated mask intensities and background intensities were corrected for instrument noise before resorufin and mCherry signal-to-background ratios (S/N) were calculated as:

$$S / N = \frac{I - N_{Inst}}{N_{cells} - N_{Inst}}$$

For each mask, the corrected YFP and mCherry intensities were converted to protein concentrations using the wedge measurements above, assuming linearity between concentration and intensity and assuming cell thickness to be uniformly 5 μm . Using this method, we determined that 0.5 μM intracellular mCherry generated a 2:1 signal-to-noise ratio in imaging.

Analysis of orthogonal resorufin and coumarin ligation *in vitro* by HPLC (Fig. S11A)

Reactions were assembled with 1 μM resorufin ligase or coumarin ligase, 400 μM resorufin **2** or coumarin, 200 μM LAP (GFEIDKVWYDLDA), 2 mM ATP, and 5 mM $\text{Mg}(\text{OAc})_2$ in DPBS containing 10% (v/v) glycerol and reacted at room temperature for 90 min. Reactions were then quenched with a final concentration of 50 mM ethylenediaminetetraacetic acid and subsequently analyzed by HPLC according to General Methods.

Cellular two-color labeling with resorufin **2**-AM₂ and coumarin-AM₂ (Fig. S11B-C)

Two pools of HEK cells grown in a 6-well plate were transfected separately. Pool 1 was transfected with resorufin ligase and a nuclear localized LAP-YFP in a 1:1 ratio of plasmids. Pool 2 was transfected with coumarin ligase (^{W37V}LplA) and nuclear excluded LAP-YFP in a 1:10 ratio of plasmids. 18 hr after transfection, the cells were lifted by trypsin digest, mixed, then re-plated onto glass coverslips pre-treated with human fibronectin. 24 hr after re-plating the cells were rinsed twice with serum-free MEM, then treated with MEM containing 5 μM resorufin **2**-AM₂ and 20 μM coumarin-AM₂ (**2**) in MEM for 10 min. at 37 °C. The cells were then rinsed three times with complete growth medium. Dye washout occurred in the same medium over 40 min. at 37 °C. Cells were then imaged live in DPBS.

References

1. Fujiwara K et al. (2010) Global conformational change associated with the two-step reaction catalyzed by Escherichia coli lipoate-protein ligase A. *J Biol Chem* 285:9971–9980.
2. Uttamapinant C et al. (2010) A fluorophore ligase for site-specific protein labeling inside living cells. *Proc Natl Acad Sci* 107:10914–10919.
3. Puthenveetil S, Liu DS, White KA, Thompson S, Ting AY (2009) Yeast display evolution of a kinetically efficient 13-amino acid substrate for lipoic acid ligase. *J Am Chem Soc* 131:16430–16438.
4. Fujiwara K et al. (2005) Crystal structure of lipoate-protein ligase A from Escherichia coli. Determination of the lipoic acid-binding site. *J Biol Chem* 280:33645–33651.
5. Fernández-Suárez M et al. (2007) Redirecting lipoic acid ligase for cell surface protein labeling with small-molecule probes. *Nat Biotechnol* 25:1483–1487.
6. Bueno C et al. (2002) The Excited-State Interaction of Resazurin and Resorufin with Amines in Aqueous Solutions. Photophysics and Photochemical Reaction. *Photochem Photobiol* 76:385–390.

7. Adams SR et al. (2002) New Biarsenical Ligands and Tetracysteine Motifs for Protein Labeling in Vitro and in Vivo: Synthesis and Biological Applications. *J Am Chem Soc* 124:6063–6076.
8. Cohen JD, Thompson S, Ting AY (2011) Structure-Guided Engineering of a Pacific Blue Fluorophore Ligase for Specific Protein Imaging in Living Cells. *Biochemistry (Mosc)* 50:8221–8225.
9. Yao JZ et al. (2012) Fluorophore Targeting to Cellular Proteins via Enzyme-Mediated Azide Ligation and Strain-Promoted Cycloaddition. *J Am Chem Soc* 134:3720–3728.
10. Liu DS, Phipps WS, Loh KH, Howarth M, Ting AY (2012) Quantum Dot Targeting with Lipoic Acid Ligase and HaloTag for Single-Molecule Imaging on Living Cells. *ACS Nano* 6:11080–11087.
11. Dunbrack RL Jr, Karplus M (1993) Backbone-dependent rotamer library for proteins. Application to side-chain prediction. *J Mol Biol* 230:543–574.
12. Kuhlman B et al. (2003) Design of a novel globular protein fold with atomic-level accuracy. *Science* 302:1364–1368.
13. Leaver-Fay A, Snoeyink J, Kuhlman B (2008) in *Bioinformatics Research and Applications*, Lecture Notes in Computer Science., eds Măndoiu I, Sunderraman R, Zelikovsky A (Springer Berlin Heidelberg), pp 343–354. Available at: http://link.springer.com/chapter/10.1007/978-3-540-79450-9_32 [Accessed July 18, 2013].
14. Meiler J, Baker D (2006) ROSETTALIGAND: protein-small molecule docking with full side-chain flexibility. *Proteins* 65:538–548.
15. Otwinowski Z, Minor W (1997) in *Methods in Enzymology*, ed Charles W. Carter J (Academic Press), pp 307–326. Available at: <http://www.sciencedirect.com/science/article/pii/S007668799776066X> [Accessed August 16, 2013].
16. McCoy AJ et al. (2007) Phaser crystallographic software. *J Appl Crystallogr* 40:658–674.
17. Emsley P, Cowtan K (2004) Coot: model-building tools for molecular graphics. *Acta Crystallogr D Biol Crystallogr* 60:2126–2132.
18. Adams PD et al. (2010) PHENIX: a comprehensive Python-based system for macromolecular structure solution. *Acta Crystallogr D Biol Crystallogr* 66:213–221.
19. Shaner NC, Steinbach PA, Tsien RY (2005) A guide to choosing fluorescent proteins. *Nat Methods* 2:905–909.